

## Chapter 5

### Lowest Landau Level [4]

#### 5.1 Introduction

Rotating Bose-Einstein condensates provide a conceptual link between the physics of trapped gases and the physics of condensed matter systems such as superfluids, type-II superconductors and quantum Hall effect (QHE) materials. In all these systems, striking counterintuitive effects emerge when an external flux penetrates the sample. For charged particles this flux can be provided by a magnetic field, leading to the formation of Abrikosov flux line lattices in type-II superconductors [74], or in QHE systems to the formation of correlated electron-liquids and composite quasiparticles made of electrons with attached flux quanta [90]. For neutral superfluids, the analog to a magnetic field is a rotation of the system, which similarly spawns vortices [91]. In rotating atomic BECs, the creation of large ordered Abrikosov lattices of vortices [22, 24, 23, 25] has recently become possible.

Here we examine the vortex lattice of harmonically trapped BECs approaching the high rotation limit, when the centrifugal force nearly cancels the radial confining force. The formal analogy of neutral atoms in this limit with electrons in a strong magnetic field has led to the prediction that quantum-Hall like properties should emerge in rapidly rotating atomic BECs [37]. In particular, the single-particle energy states, in the rotating frame, organize into Landau levels (see figure 5.1), and if interactions are weaker than the cyclotron energy (approximately the energy splitting between Landau

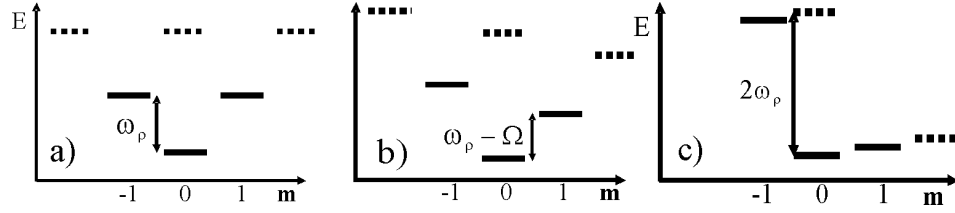


Figure 5.1: Harmonic oscillator states in the rotating frame as one approaches the lowest Landau level. Image a) shows the non-rotating case. With moderate condensate rotation the positive/negative  $m$  harmonic oscillator states shift down/up in energy as seen in image b). As condensate rotation rate ( $\Omega$ ) approaches the trap frequency ( $\omega_\rho$ ) the harmonic oscillator states form bands, or Landau levels, as in image c). The condensate becomes confined to the lowest Landau level if the chemical potential drops below the Landau level splitting ( $2\omega_\rho$ ).

levels), the near-degenerate states of the lowest Landau level (LLL) are primarily occupied. For rotating bosons in the LLL, two regimes have been identified, distinguished by the filling factor  $\nu \equiv N_p/N_v$ , i.e., the ratio of the number of particles ( $N_p$ ) to vortices ( $N_v$ ). For high filling factors (always  $\geq 500$  in our system), the condensate is in the lowest Landau level regime [35, 19, 36], but mean-field theory is still a valid way to deal with interactions. In this state the condensate still forms an ordered vortex lattice ground state. With decreasing filling factor, the elastic shear strength of the vortex lattice decreases, which is reflected in very low frequencies of long-wavelength transverse lattice excitations (Tkachenko oscillations [28, 84, 29, 43, 30, 31, 83, 85, 33, 86, 32])<sup>1</sup>. For filling factors around  $\nu \approx 10$ , the shear strength is predicted to drop sufficiently for quantum fluctuations to melt the vortex lattice[37, 38]. For smaller  $\nu$  there exists a variety of strongly correlated vortex liquid states similar to those in the Fermionic fractional QHE [37]. Starting from the Laughlin state, one can then even create excitations that obey fractional statistics [39].

In this chapter we report the observation of rapidly rotating BECs in the lowest Landau level, and provide evidence that the elastic shear strength of the vortex lattice

<sup>1</sup> Ref. [84] measured Tkachenko frequencies that showed deviations from existing TF-limit theory valid at low rotation [28] (also shown in §4.3). These were resolved in subsequent theoretical work [29, 30, 31].

drops substantially as the BEC enters the lowest Landau level regime [29]. This effect is a precursor to the predicted quantum melting of the lattice at lower filling factors. Our rapidly rotating condensates spin out into a pancake shape and approach the quasi-two-dimensional regime. We observe a corresponding cross-over in the spectrum of breathing excitations along the axial direction. The high rotation limit has been studied experimentally in Ref. [92], focusing on effects of a rotating trap anisotropy, which is not present in our setup, and in Ref. [93] where the addition of a quartic term to the trapping potential led to a loss of vortex visibility.

## 5.2 Experiment

These experiments take place in an axially symmetric harmonic trap with oscillation frequencies  $\{\omega_\rho, \omega_z\} = 2\pi\{8.3, 5.3\}$  Hz. Using an evaporative spin-up technique described in §2.1 we create condensates containing up to  $5.5 \times 10^6$   $^{87}\text{Rb}$  atoms in the  $|F = 1, m_F = -1\rangle$  state, rotating about the vertical, z axis, at a rate  $\tilde{\Omega} = 0.95$  ( $\tilde{\Omega} \equiv \Omega/\omega_\rho$  is the rotation rate  $\Omega$  scaled by the centrifugal rotation limit,  $\omega_\rho$ , for a harmonically trapped gas). To further approach the limit  $\tilde{\Omega} \rightarrow 1$ , we employ an optical spin-up technique, where the BEC is illuminated uniformly with laser light, and the recoil from spontaneously scattered photons removes atoms from the condensate. Since the condensate is optically thin to the laser light, atoms are removed without position or angular-momentum selectivity, such that angular momentum per particle is unchanged. Atom loss leads to a small decrease in cloud radius which, through conservation of angular momentum, increases  $\tilde{\Omega}$ . Over a period of up to 2 seconds we decrease the number of BEC atoms by up to a factor of 100, to  $5 \times 10^4$ , while increasing<sup>2</sup>  $\tilde{\Omega}$  from 0.95 to more than 0.99. At this point, further reduction in number degrades the quality of images unacceptably. Ongoing evaporation is imposed to retain a quasi-pure BEC with

---

<sup>2</sup> Rotation rates are accurately determined by comparing the measured BEC aspect ratio to the trap aspect ratio (see e.g. [40]). At our lowest values of  $\Gamma_{2D}$  we correct for quantum-pressure contributions to axial size.

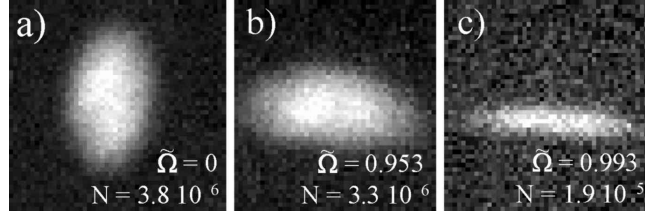


Figure 5.2: Side view images of BECs in trap. (a) Static BEC. The aspect ratio  $R_z/R_\rho = 1.57$  ( $N = 3.8 \times 10^6$  atoms) resembles the prolate trap shape. (b) After evaporative spin-up,  $N = 3.3 \times 10^6$ ,  $\tilde{\Omega} = 0.953$ , (c) evaporative plus optical spin-up,  $N = 1.9 \times 10^5$ ,  $\tilde{\Omega} = 0.993$ . Due to centrifugal distortion the aspect ratio is changed by a factor 8 compared to (a).

no discernible thermal cloud.

### 5.3 Breathing mode spectrum in the lowest Landau level

With increasing rotation, centrifugal force distorts the cloud into an extremely oblate shape [see figure 5.2] and reduces the density significantly - thus the BEC approaches the quasi-two-dimensional regime. For the highest rotation rates we achieve, the chemical potential  $\mu$  is reduced close to the axial oscillator energy,  $\Gamma_{2D} \equiv \frac{\mu}{2\hbar\omega_z} \approx 1.5$ , and the gas undergoes a cross-over from interacting- to ideal-gas behavior along the axial direction.

To probe this cross-over, we excite the lowest order axial breathing mode over a range of rotation rates. For a BEC in the axial Thomas-Fermi regime, an axial breathing frequency  $\omega_B = \sqrt{3}\omega_z$  has been predicted in the limit  $\tilde{\Omega} \rightarrow 1$  [40], whereas  $\omega_B = 2\omega_z$  is expected for a non-interacting gas.

To excite the breathing mode, we jump the axial trap frequency by 6%, while leaving the radial frequency unchanged (within  $< 0.5\%$ ). To extract the axial breathing frequency  $\omega_B$ , we take 13 nondestructive in-trap images of the cloud, perpendicular to the axis of rotation. From the oscillation of the axial Thomas-Fermi radius<sup>3</sup> in time we obtain  $\omega_B$ . Rotation rates are obtained from the aspect ratio by averaging over

<sup>3</sup> For the smallest values  $\Gamma_{2D}$ , the axial density profile is slightly better fitted by a Gaussian. To avoid bias however we fit all data assuming a TF profile.

all 13 images to eliminate the effect of axial breathing. As shown in figure 5.3(a), we do indeed observe a frequency cross-over from  $\omega_B = \sqrt{3}\omega_z$  to  $\omega_B = 2\omega_z$  as  $\tilde{\Omega} \rightarrow 1$ . To quantify under which conditions the cross-over occurs, we plot the same data vs.  $\Gamma_{2D}$  [figure 5.3(b)], where the chemical potential is determined from the measured atom number, the rotation rate and the trap frequencies. For  $\Gamma_{2D} < 3$ , the ratio  $\omega_B/\omega_z$  starts to deviate from the predicted hydrodynamic value, and approaches 2 for our lowest  $\Gamma_{2D} \approx 1.5$ .

As  $\tilde{\Omega} \rightarrow 1$ , the dynamics in the radial plane are also affected. For the highest rotation rates, interactions become sufficiently weak that the chemical potential  $\mu$  drops below the cyclotron energy  $2\hbar\Omega$ , which is only a few percent smaller than the Landau level spacing  $2\hbar\omega_\rho$ . Then,  $\Gamma_{LLL} \equiv \frac{\mu}{2\hbar\Omega} < 1$ , and the condensate primarily occupies single-particle states in the LLL. These form a ladder of near-degenerate states, with a frequency splitting of  $\epsilon = \omega_\rho - \Omega$ . The number of occupied states is  $N_{LLL} \approx \frac{\mu}{\hbar\epsilon}$ . We are able to create condensates with  $\Gamma_{LLL}$  as low as 0.6, which occupy  $N_{LLL} \approx 120$  states, with a splitting  $\epsilon < 2\pi \times 0.06$  Hz. In this regime of near-degenerate single-particle states a drastic decrease of the lattice's elastic shear strength takes place. The elastic shear modulus,  $C_2$ , is predicted by Baym [29] to decrease with increasing rotation rate from its value in the “stiff” Thomas-Fermi (TF) limit,  $C_2^{TF} = n_{(\Omega)}\hbar\Omega/8$  (where  $n_{(\Omega)}$  is the BEC number density) to its value in the mean-field quantum Hall regime, of  $C_2^{LLL} \approx 0.16 \times \Gamma_{LLL} \times C_2^{TF}$ . We directly probe this shear strength by exciting the lowest order azimuthally symmetric lattice mode (  $(n = 1, m = 0)$  Tkachenko mode [28, 84, 29]). Its frequency  $\omega_{(1,0)} \sim \sqrt{C_2}$  is expected to drop by a factor  $\approx 2.5$  below the TF prediction when  $\Gamma_{LLL} = 1$ .

#### 5.4 Tkachenko spectrum in the lowest Landau level

Our excitation technique for Tkachenko modes has been described in §4.2. Here the lower interaction strength of the condensates makes it preferable to use the focused,

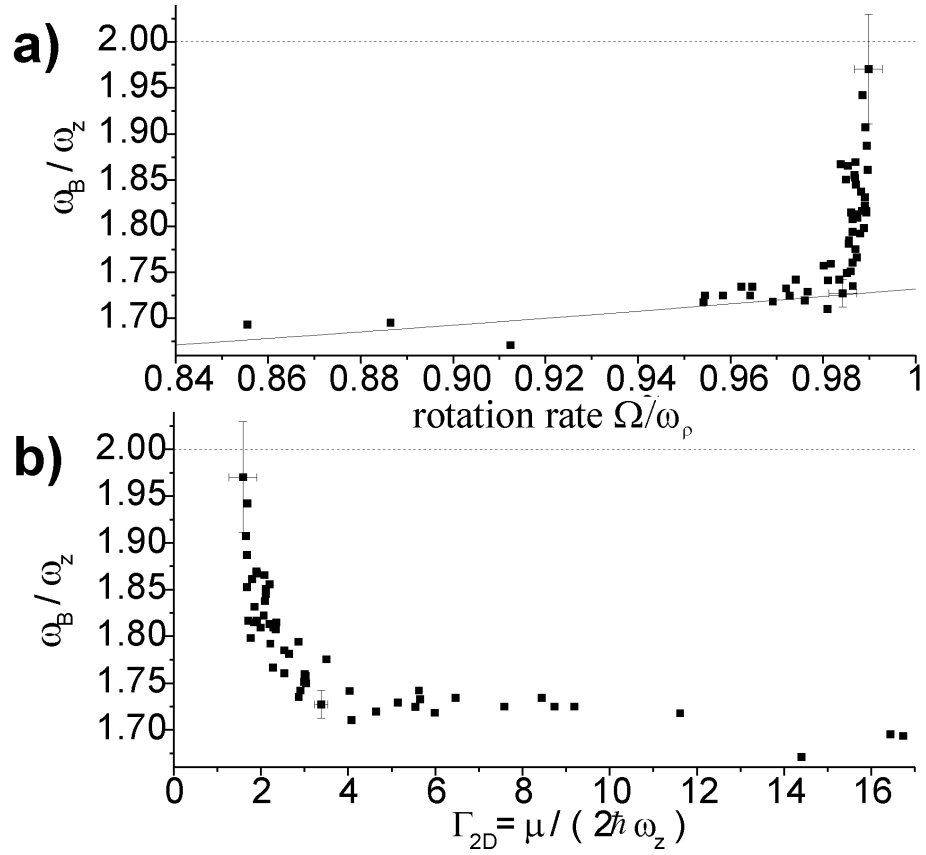


Figure 5.3: Measured axial breathing frequency  $\omega_B/\omega_z$  (a) as a function of rotation rate  $\tilde{\Omega}$  and (b) vs.  $\Gamma_{2D}$ . Solid line: Prediction for the hydrodynamic regime [40]; Dashed line: ideal gas limit. For  $\tilde{\Omega} > 0.98$  ( $\Gamma_{2D} < 3$ ) a cross-over from interacting- to ideal-gas behavior is observed. Representative error bars are shown for two data points.

red-detuned laser (850 nm). This laser draws atoms into the center, and Coriolis force diverts the atoms' inward motion into the lattice rotation direction. The vortex lattice adjusts to this distortion, and after we turn off the beam, the lattice elasticity drives oscillations at the frequency  $\omega_{(1,0)}$ . We observe the oscillation by varying the wait time after the excitation, and then expanding the condensate before imaging the vortex lattice along the z-axis [see figure 5.4(a),(b)]. In figure 5.4(c), we compare the measured frequencies  $\omega_{(1,0)}$  to the predictions of Ref. [29] for the TF limit and for the mean-field quantum Hall regime. For  $\tilde{\Omega} < 0.98$  ( $\Gamma_{LLL} > 3$ ), the frequency  $\omega_{(1,0)}$  follows the prediction for the TF regime, whereas by  $\tilde{\Omega} = 0.990$  ( $\Gamma_{LLL} = 1.5$ ),  $\omega_{(1,0)}$  has dropped to close to the prediction for the LLL, thus providing evidence for the cross-over to the lower shear modulus  $C_2$  predicted for the LLL.

While we are able to produce clouds with  $\Gamma_{LLL}$  measured to be substantially lower than  $\Gamma_{LLL} = 1.5$ , we are unable to accurately measure Tkachenko frequencies under these extreme conditions, due at least in part to the very weakness of  $C_2$ . The Tkachenko mode frequencies become so low that it takes multiple seconds to track even a quarter oscillation [figure 5.4(a),(b)]. Concurrently, the very weak shear strength means that even minor perturbations to the cloud can cause the lattice to melt and the individual cores to lose contrast<sup>4</sup> in a matter of seconds. These perturbations can result from residual asymmetry of the magnetic trapping potential, or from spatial structure in the optical beam used to reduce the atom number, or perhaps from thermal fluctuations. In contrast, for a “stiff” cloud of  $3 \times 10^6$  atoms at  $\tilde{\Omega} = 0.95$  ( $\Gamma_{LLL} \approx 7$ ) we observe that the lattice remains ordered, and  $\tilde{\Omega}$  can be kept constant, over the entire  $1/e$  lifetime of the BEC ( $\approx 3$  minutes).

---

<sup>4</sup> Melting and loss of contrast are also reported in Ref. [93].

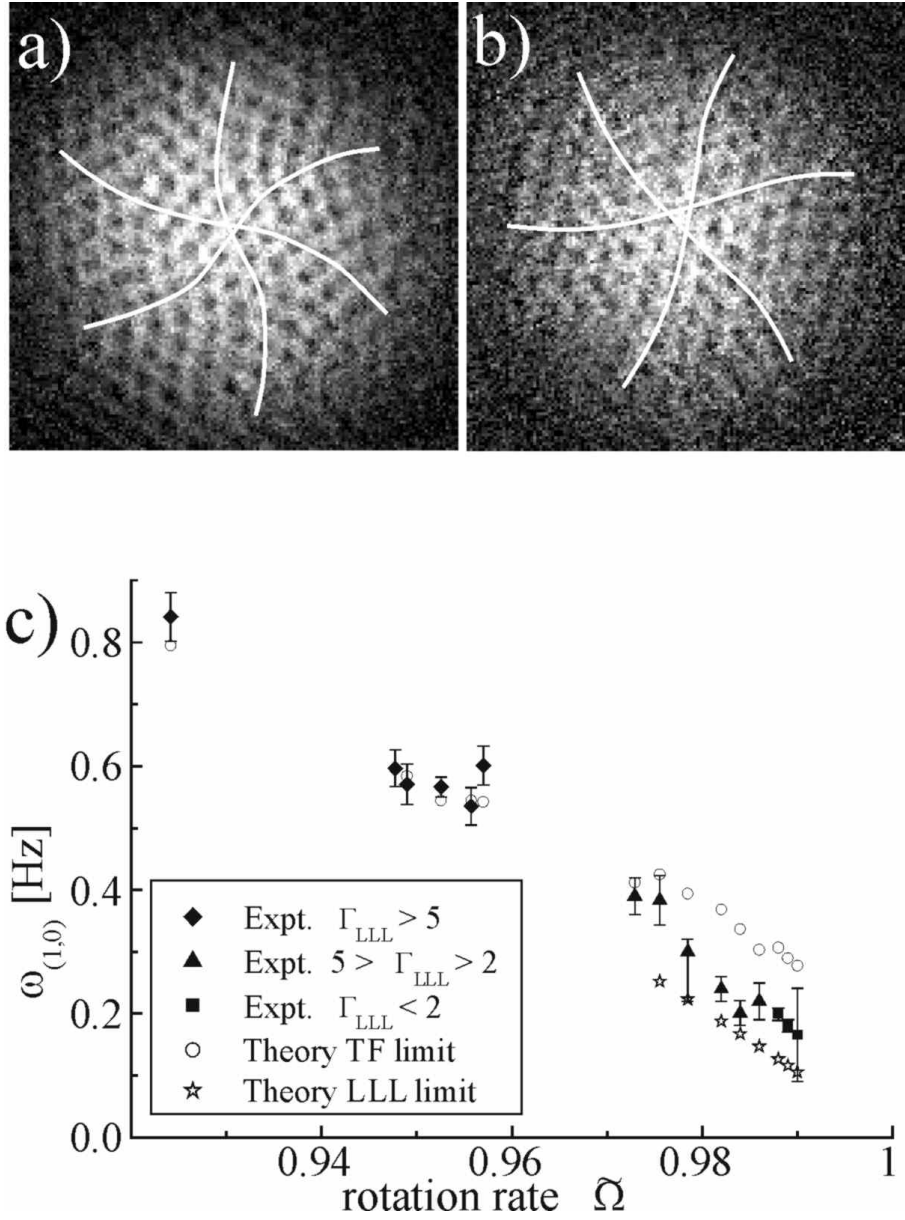


Figure 5.4: (a), (b) Tkachenko mode at  $\Gamma_{LLL} = 1.2$  ( $N = 1.5 \times 10^5$ ,  $\tilde{\Omega} = 0.989$ ): (a) directly after excitation, (b) after 1 sec - the lattice oscillation has not yet completed 1/4 cycle. (c) Comparison of measured Tkachenko mode frequency  $\omega_{(1,0)}$  (solid symbols) vs.  $\tilde{\Omega}$  to theory, using vortex lattice shear modulus  $C_2^{TF}$  in the Thomas-Fermi (TF) limit (circles), and  $C_2^{LLL}$  in the mean-field quantum Hall regime (stars). Note that both  $N$  and  $\Gamma_{LLL}$  decrease as  $\tilde{\Omega}$  increases. For  $\Gamma_{LLL} \approx 3$  (reached at  $N = 7.8 \times 10^5$ ,  $\tilde{\Omega} \approx 0.978$ ) the data cross over from the TF to the quantum Hall prediction.

## 5.5 Fractional core area

The fractional condensate area occupied by the vortex cores, as one approaches the lowest Landau level, is also a quantity that has been of much theoretical interest [19, 36, 45, 46]. It is argued by Fischer and Baym [19] and Baym and Pethick [36] that the fractional core area reaches a limiting value as one enters the LLL regime. A corollary to this argument is that fractional core area is a reasonable way to monitor the transition to the lowest Landau level regime. We examine this saturation with experimental and numerical work, which we can push further into this regime than we can achieve experimentally. Additionally we examine some of the systematic errors that can affect the experimental data. To this end numerical calculations were performed as previously described (§2.6), for  $3 \times 10^6$ ,  $5 \times 10^5$ , and  $1 \times 10^5$  atoms, and for rotations ranging from  $\Omega/\omega_\rho = 0.15$  to 0.998. For the experimental data, actual condensates were generated over a similar range with  $\Omega/\omega_\rho = 0.15$  to 0.98 and  $N = 4 - 50 \times 10^5$ . The numerical data as well as the experimental data are fit in the same manner as described in §2.3.

We define the fractional area,  $\mathcal{A}$ , occupied by the vortices to be  $\mathcal{A} = n_v \pi r_v^2$ , where  $n_v$  is the areal density of vortices and  $r_v^2$  is the 2D RMS vortex core radius. To determine a theoretical value for  $r_v$ , we perform a numerical simulation of the Gross-Pitaevskii (GP) equation of a BEC containing an isolated vortex. We obtain  $r_v = 1.94 \times \xi$  with  $\xi = (8\pi n a)^{-\frac{1}{2}}$ , where  $a$  is the scattering length and  $n$  is the density<sup>5</sup>.

Ignoring density inhomogeneity effects (discussed later), and in the limit of many vortices, the expected vortex density  $n_v$  is  $m\Omega/(\pi\hbar)$ . The resulting prediction for  $\mathcal{A}$  can be expressed as  $\mathcal{A} = 1.34 \times \Gamma_{LLL}^{-1}$ . This value exceeds unity for  $\Gamma_{LLL} < 1.34$ , which has led to the prediction that vortices should merge as the condensate enters the LLL

<sup>5</sup> The density  $n = 7/10 n_{peak}$  is density-weighted along the rotation axis and is radially averaged over the vortex cores within 1/2 the TF radius, as it is only in this region that we fit the observed vortex cores.

regime. An alternate treatment from Baym and Pethick [36] predicts that  $\mathcal{A}$  saturates at 0.225 as the vortices go from a Thomas-Fermi profile to the profile of a LLL wave function. Our numerical data for  $\mathcal{A}$ , together with experimental points, are plotted in figure 5.5 (a,b). For  $\Gamma_{LLL}^{-1} < 0.1$ , the data agree reasonably well with the Thomas-Fermi result. For larger  $\Gamma_{LLL}^{-1}$ , the data clearly show a smooth transition to the LLL regime, and a saturation of  $\mathcal{A}$  at the LLL limit.

The experimental data in figure 2.8(b) tend to lie above the numerical data. This is likely due to the fact that there are many systematic errors that tend to bias the data toward larger core size. Consequently, we tend to overestimate the core size. Of all the systematic errors we have studied, axial expansion of the cloud during the expansion process is by far the most prevalent. Figure 2.8(c) demonstrates the dangers of axial expansion in this measurement. For the data presented, the condensate undergoes a factor of 2-3 in axial expansion, and we see a corresponding increase in  $\mathcal{A}$ . This clearly illustrates the importance in suppressing axial expansion for these measurements. It is interesting to note that with our rapid axial expansion the fractional core area can overshoot the LLL limit, which in principle should still be valid in the limit of adiabatic expansion.

## 5.6 Vortex core density profile

We can also observe the transition to the LLL regime in the numerical data by examining the shape of the condensate vortex cores. In the Thomas-Fermi regime, the vortex-core density profile is well described by the form  $n(r) = (r/\sqrt{2\xi^2 + r^2})^2$  [94], where  $r$  is measured from the vortex center. Alternatively in the LLL regime, the core is no longer dictated by the interactions but rather by kinetic energy considerations. In this case, within the Wigner-Seitz unit cell, the vortex is thought [36] to have a simple oscillator p-state structure  $n(r) = ((Cr/b) \cdot \exp[-r^2/2l^2])^2$  for  $0 \leq r \leq l$ , where  $C$  is a normalization constant, and  $l$  is the radius of the Wigner-Seitz unit cell and is

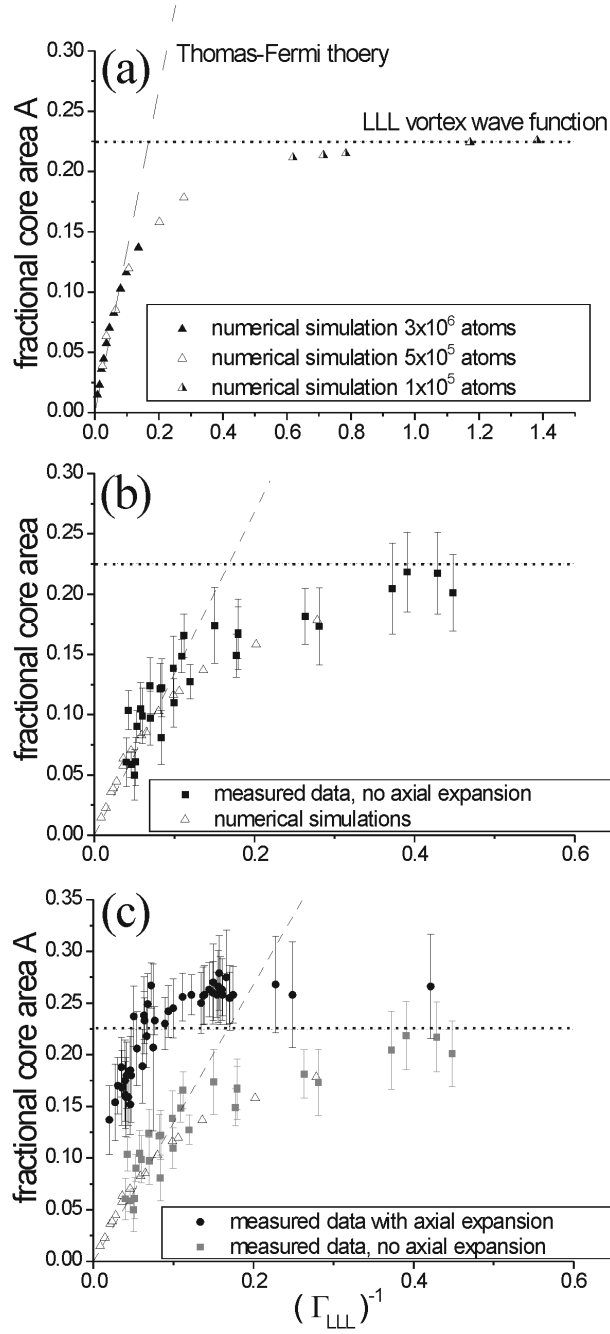


Figure 5.5: Fractional condensate area occupied by vortex cores ( $\mathcal{A}$ ) as a function of  $\Gamma_{LLL}^{-1} = 2\hbar\Omega/\mu$ , the inverse lowest Landau level parameter. Plot (a) shows a smooth transition in the numerical data from the Thomas-Fermi limit where  $\mathcal{A}$  is linear in  $\Gamma_{LLL}^{-1}$  to the LLL limit where  $\mathcal{A}$  saturates. Here the Thomas-Fermi theory is represented by the dashed line and the LLL limit by the dotted line. Plot (b) is a comparison of the numerical data to experimental data. Plot (c) demonstrates the effect on the experimental measurement of allowing the condensate to expand axially during the expansion process.

related to the nearest-neighbor lattice spacing  $b$  by  $l = (\sqrt{3}/2\pi)^{1/2}b$ . Figure 5.6 is a comparison of the central vortex, in three numerically generated condensates, to both Thomas-Fermi and LLL predicted core shapes. The simulation for figure 5.6(a) was performed for  $3 \times 10^6$  atoms and  $\Omega/\omega_\rho = .15$  and is well inside the Thomas-Fermi regime ( $\Gamma_{LLL} = 117$ ). Here the density profile of the numerical data (solid line) seems to fit quite well to the Thomas-Fermi vortex form (dotted line), but the LLL form is a poor description of the vortex core (dashed line). The simulation for figure 5.6(b) was performed for  $5 \times 10^5$  atoms,  $\Omega/\omega_\rho = .95$  and  $\Gamma_{LLL} = 3.6$ . One can see from figure 5.5 that this is in the transition region. Not surprisingly both vortex forms fit about equally well. In Figs. 5.6(b) and figure 5.6(c), the vertical line represents the edge of the Wigner-Seitz unit cell at  $r = l$ . The simulation for figure 5.6(c) was performed with  $1 \times 10^5$  atoms,  $\Omega/\omega_\rho = .998$  and  $\Gamma_{LLL} = .72$ . One can see that LLL is a much better description of the vortex.

## 5.7 Condensate radial density profile

On a separate but interesting note, as we enter the LLL regime, our numerical solution of the GP equation shows that the radial profile of the overall smoothed condensate fits much better to a parabola than to the Gaussian that was originally predicted [35]. We can also confirm this experimentally by imaging clouds with  $\Gamma_{LLL}$  as small as 0.6. Images are taken in-trap, to increase signal, and after 3 sec equilibration time. Examining the radial density profile we find that these images also fit better to a TF profile than to a Gaussian, showing no signs of a cross-over in the radial density profile as the LLL is entered.

The reason the Gaussian-density-profile prediction fails to pan out can be extrapolated from data presented in the next chapter. The density-profile prediction for the radial profile in the LLL arose from an elegant argument that was based on an assumption that the vortex nodes were on a perfect triangular lattice. As was originally pointed

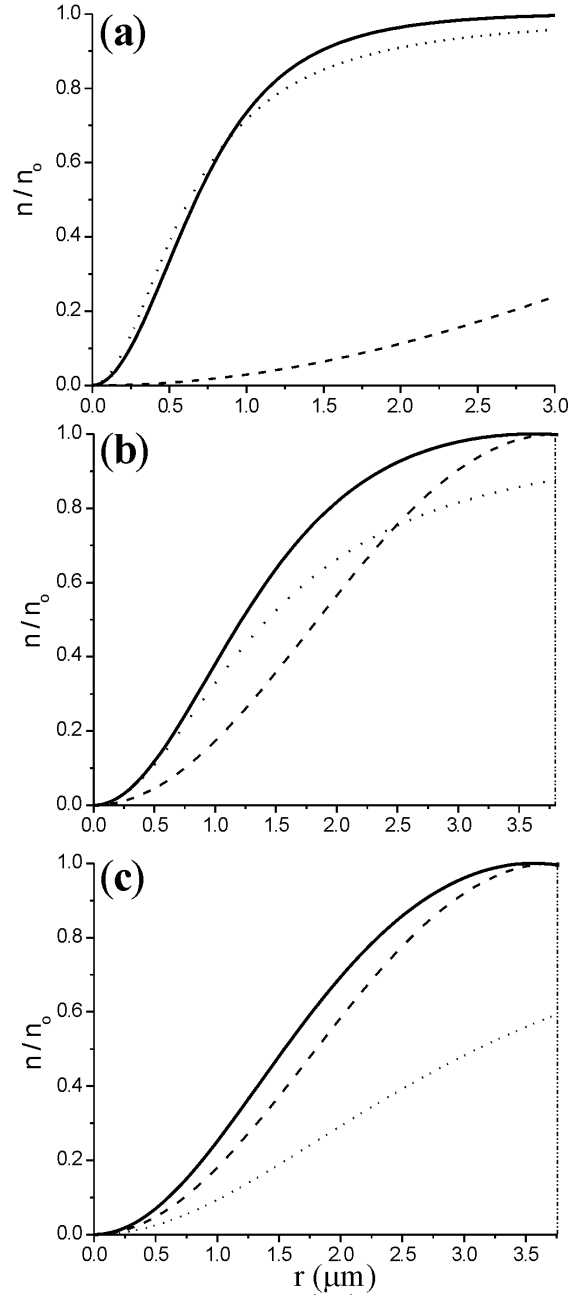


Figure 5.6: Numerically generated vortex core density profiles approaching the lowest Landau level regime. Density  $n$  is scaled by the peak density  $n_0$ . Solid lines represent the numerical result for (a)  $\Gamma_{LLL} = 117$ , (b)  $\Gamma_{LLL} = 3.6$ , (c)  $\Gamma_{LLL} = .72$ . The dashed line is the expected profile for a LLL wave function [36] given the condensate rotation. The dotted line is the expected vortex form in the Thomas-Fermi limit [94] given the condensate density. The vertical lines in figure (b) and (c) designate the edge of the Wigner-Seitz unit cell. As  $\Gamma_{LLL}$  decreases, one can see a clear transition from the interaction-dominated Thomas-Fermi regime to a LLL function where kinetic energy concerns and the vortex core spacing dictate the shape and size of the vortex.

out to us by A. H. MacDonald [43] and has been the subject of two recent theoretical works [41, 42], a slight radially dependant perturbation in the areal density of vortices is enough to convert a Gaussian density distribution into an inverted parabola. The analytic description of this perturbation in [41] (calculated in the LLL) bears a striking resemblance to the one measured in §6.2 in the Thomas-Fermi regime and also to the analytic form [44] calculated in the Thomas-Fermi regime. The surprising result of this perturbation in the areal density of vortices is that one of the most striking features of the Thomas-Fermi regime, the parabolic Thomas-Fermi density profile, still exists in the LLL regime where the condensate kinetic energy is clearly non-negligible compared to interaction energy.